


Article

A PSO-CNN-Based Deep Learning Model for Predicting Forest Fire Risk on a National Scale

Xingyue You ¹, Zhong Zheng ¹ , Kangquan Yang ^{2,*}, Liang Yu ¹, Jinbao Liu ¹, Jun Chen ¹, Xiaoning Lu ¹ and Shanyun Guo ²

¹ College of Resources and Environment, Chengdu University of Information Technology, Chengdu 610225, China; aeyifaru5@gmail.com (X.Y.); zhengzhong@cuit.edu.cn (Z.Z.); yuliang@cuit.edu.cn (L.Y.); ljb@cuit.edu.cn (J.L.); cj@cuit.edu.cn (J.C.); lxn@cuit.edu.cn (X.L.)

² Sichuan Provincial Meteorological Observatory, Chengdu 610072, China; griseldavakas5@gmail.com

* Correspondence: yangkangquan@aliyun.com; Tel.: +86-(0)-18782092468

Abstract: Forest fires have a significant impact on terrestrial ecosystems, leading to harm to biodiversity and environment. To mitigate the ecological damage caused by forest fires, it was necessary to develop prediction models of fire risk. In this study, by evolving the optimal architecture and parameters using the particle swarm optimization (PSO) algorithm, a convolutional neural network (CNN) deep learning model was proposed to predict forest fire risk on a national scale. Utilizing fire data and fire risk factors from 2001 to 2020 in China, the PSO-CNN-based deep learning model (PSO-CNN) was utilized and tested. Compared to logistic regression, random forest, support vector machine, k-nearest neighbors, and CNN models, the PSO-CNN model exhibited superior performance with an accuracy of 82.2% and an AUC value of 0.92. These results clearly highlighted the effectiveness of the PSO-CNN model in enhancing the accuracy of forest fire prediction. Furthermore, the forest fire risk prediction level estimated by the proposed model on a national scale for the entire country was mostly consistent with actual fire data distribution, indicating its potential to be used as an important direction for deep learning in forest fire prediction research.

Keywords: forest fire; convolutional neural network; particle swarm optimization; nighttime lights; China



Citation: You, X.; Zheng, Z.; Yang, K.; Yu, L.; Liu, J.; Chen, J.; Lu, X.; Guo, S. A PSO-CNN-Based Deep Learning Model for Predicting Forest Fire Risk on a National Scale. *Forests* **2024**, *15*, 86. <https://doi.org/10.3390/f15010086>

Academic Editors: Chao Ren and Maofang Gao

Received: 1 December 2023

Revised: 22 December 2023

Accepted: 29 December 2023

Published: 31 December 2023



Copyright: © 2023 by the authors. Licensee MDPI, Basel, Switzerland. This article is an open access article distributed under the terms and conditions of the Creative Commons Attribution (CC BY) license (<https://creativecommons.org/licenses/by/4.0/>).

1. Introduction

Forests play an irreplaceable role in maintaining ecosystem safety [1]. Unfortunately, the increased prevalence of global warming and extreme weather conditions has led to frequent forest fires, resulting in significant ecological damage to forested areas [2,3]. Especially in China, an average of about 1900 forest fires occurred per year during the period 2017–2021, leading to the destruction of around 13,000 hectares of forest. Therefore, researchers have made significant efforts in the field concerning forest fires, including research on forest fire prediction [4,5], forest fire spread [6,7], and burn severity of forest fires [8,9]. This study aimed to carry out research related to forest fire prediction in order to mitigate the ecological losses caused by fires.

In general, forest fire was influenced by various risk factors, e.g., combustible materials, meteorological variables, and human activities [10,11]. These factors were typically characterized by multiple sources and formats, making it challenging to create quantitative models for characterizing fire risk. As a result, current research efforts have focused on the development of advanced quantitative methods. For example, Lozano et al. [12] applied multi-temporal Landsat data to model fire occurrence probability using a logistic regression model in Mediterranean ecosystems. Similarly, in order to improve the effectiveness of fire prediction, Catry et al. [13] used logistic regression models to determine the likelihood of wildfire ignition in mainland Portugal, revealing that human activities, land cover, and elevation were critical determinants of fire ignition. Furthermore, based on a study of

the density of forest fire occurrence, Wu et al. [14] combined historical ignition and kernel density estimation to deduce fire-occurrence density in Chinese boreal forests based on random forest. And then, the effect of differences in space on the occurrence of fires was taken into account. Rodrigues et al. [15] introduced geographically weighted logistic regression to model the varying spatial relationships between variables, recognized as spatial heterogeneity.

As machine learning continues to advance, it has garnered significant attention from numerous researchers in the forest fires field, e.g., Tien Bui et al. [16] presented a hybrid artificial intelligence approach using a GIS database to consider the forest fire susceptibility of tropical forests in the province of Vietnam. Moreover, Ngoc Thach et al. [17] conducted an analysis of three advanced models (support vector machine classifier, random forest, multilayer perceptron neural network) in wildfire spatial pattern. Unlike the above models, Sevinc [18] employed the k-means clustering algorithm using 11 risk factors for the preparation of forest fire risk assessment in Turkey. Zheng et al. [19] further proposed a new machine learning model based on the ant-miner algorithm to solve multivariable and non-linear problems.

Deep learning has emerged as a powerful tool in forest fire research. For instance, Satir et al. [20] used artificial neural network model to map forest fire probability in Upper Seyhan Basin (USB) in Turkey. Similarly, Zhang et al. [21] and Zhang et al. [22] utilized convolutional neural networks to predict fire occurrences. Additionally, Nguyen et al. [23] employed hybrid models (deep neural network, hunger games search and grasshopper optimization algorithm, etc.) to conduct sensitivity analysis on forest fires. As an advanced deep learning model, the convolutional neural network (CNN) has gained widespread popularity due to its effective handling of data from multiple sources. Previous studies have successfully used it for fire detection [24–26], remotely sensed image classification [21,27], and water quality prediction [28]. Consistent with this trend, the CNN model was supposed to be well-suited for predicting forest fire risk as well.

However, the network parameters of traditional CNN model were trained based on researcher experience, leading to a high potential for errors during the training process. As an automated method for optimizing parameters, particle swarm optimization (PSO) was preferred for optimization problems due to its simple formulation, few parameters, and ease of computation [29]. It utilized a chaos-based initialization technique to generate uniformly distributed particles and applies inertia-like weights to balance the exploration [30]. Therefore, the PSO algorithm was employed in this study to improve the efficiency of traditional CNN model. The main purposes of this study were as follows:

- (1) A model based on the traditional CNN deep learning algorithm was used for predicting forest fire risk in this study.
- (2) By utilizing the PSO algorithm to optimize the structure and parameters of CNN model, a PSO-CNN-based model (PSO-CNN) was proposed to predict forest fire risk on a national scale.
- (3) The performance of PSO-CNN was further tested over a long time period (from 2001 to 2020 year) and compared with certain models (i.e., logistic regression model, random forest model, support vector machine and k-nearest neighbors).

The rest of the article is structured as follows. Section 2 outlines the study area and data. We describe the methodology of this study in Section 3. Results are presented in Section 4 and the discussion is given in Section 5. Section 6 provides conclusions based on the results and discussion.

2. Data and Data Processing

2.1. Study Area

We conducted the study in China, a vast country located in the eastern region of Asia and along the west coast of the Pacific Ocean. The terrain in China varies with a stepped distribution, being higher in the west and lower in the east. The country covers an area of approximately 9.6 million km² and spans approximately 5000 km from the east to the

west, resulting in diverse temperature and precipitation patterns. There are two major climate types: the monsoon climate in the eastern region and the temperate continental climate in the northwestern region. China's vegetation comprises temperate grasslands, temperate deserts, tropical rain forests, evergreen broad-leaved forests, deciduous broad-leaved forests, and alpine meadows. Given the vast size of China, the great climatic variation, and the fact that it is home to the largest subtropical forests in the world, forest fires occur frequently in the country [31–33].

2.2. Fire Data

The input of this study requires long-term, continuous, and stable monitoring data, and only moderate resolution imaging spectroscopy (MODIS) products are able to fulfill this condition. Therefore, we employed the daily fire mask product of MOD14A1 in China from the year 2001 to 2020. The MOD14A1 product was widely used for modeling the forest fire risk [34–39]. This product provides the spatial distribution of forest fires at a resolution of 1 km, along with other information such as fire time and confidence levels. There were 138,664 forest fires recorded from 2001 to 2020. However, those with a confidence level of 9 were filtered to ensure data reliability. The filtered data were then overlaid with land cover type datasets (MCD12Q1) to exclude temperature anomaly data from non-forested areas. Thus, 25,434 forest fires during the period from 2001 to 2020 were analyzed in this study.

In order to train the model effectively, it was necessary to partition the fire data into two distinct segments: one comprising 70% of fire data for training, and the other comprising 30% of fire data for testing. During the partitioning process, non-fire segments were also generated at a 1:1.5 ratio, providing balance to the dataset required for this proposed model [40]. The final dataset contains a total of 63,586 samples. A more detailed visualization of fires' spatial distribution from 2001 to 2020 and the number of fires per year in China were displayed (see Figure 1).

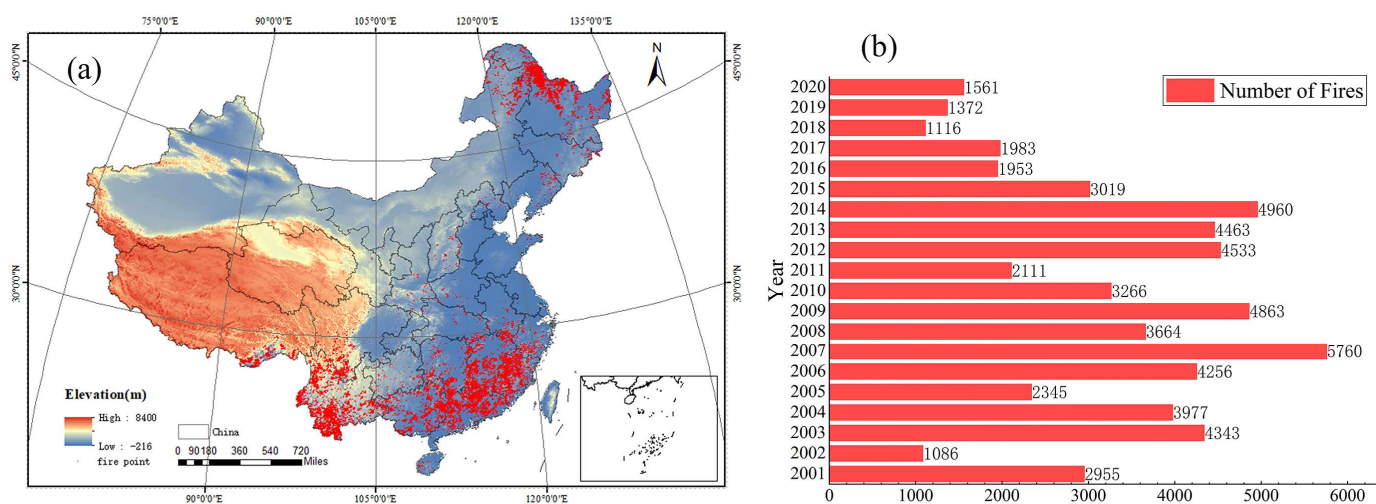


Figure 1. Forest fire in China from 2001–2020. The red dots in (a) show the distribution of all fire points in the China region from 2001 to 2020. The bars in (b) represent the number of fire point data for each year.

2.3. Fire Risk Factors

In some reported studies [41–44], fire risk factors commonly include topography, climate, combustibles and human activity. Therefore, eleven variables were taken into consideration for this study. These variables included elevation, slope, aspect, normalized difference vegetation index (NDVI), normalized multi-band drought index (NMDI), land cover, temperature, relative humidity, precipitation, wind and nighttime lights. Detailed information about the variables could be found (Table 1). Additionally, due to the challenges of obtaining natural fire variables, such as long-term thunderstorm activity, the effect of

these were not considered in this study. In summary, there are a total of 63,586 sets of risk factors, which is the same as the fire data. The distribution of these data can be observed (see Figure 2). In addition, Figure 3 provides a visual representation of the spatial distribution of these variables.

Table 1. Unit and preprocessing methods and sources for the fire risk factors dataset.

Data	Unit	Method	Source
Topography			
Elevation	m	GIS mapping	Geospatial Data Cloud
Slope	degree		
Aspect	degree		
Climate			
Temperature	°C	IDW interpolation	National Meteorological Information Center
Relative Humidity	%		
Precipitation	mm		
Wind	m/s		
Combustibles			
NDVI	-	GIS mapping	Geospatial Data Cloud
NMDI	-		
Land Cover	-	-	LAADS DAAC
Human activity			
Nighttime lights	degree	Euclidian distance	DMS/OLS; VIRRS

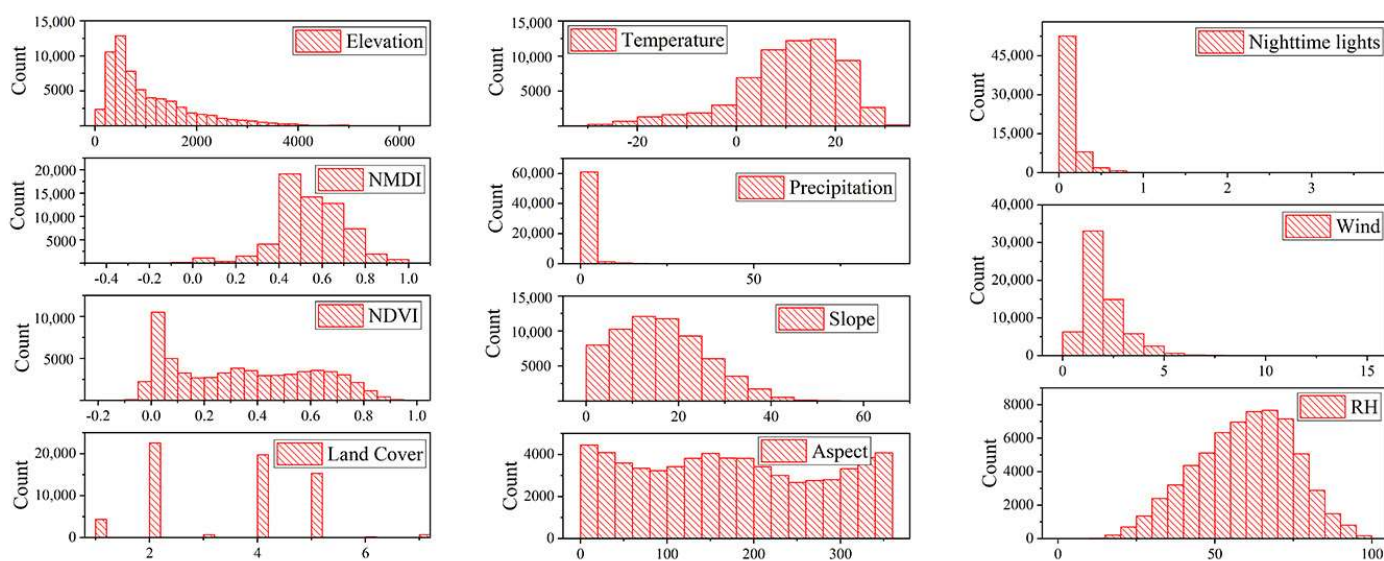


Figure 2. Distribution of risk factor data. Each of these bars represents the distribution of data for the corresponding risk factor and the corresponding number of bars.

Topographical factors have a significant impact on forest fire ignition conditions [45,46]. Hence, three topography variables including elevation, slope, and aspect were taken as inputs to develop the proposed model in this study. These variables were calculated using the digital elevation model (DEM) of China. The DEM data with a spatial resolution of 90 m were obtained from the “Geospatial Data Cloud” platform (<https://www.gscloud.cn/>), accessed on 1 July 2021.

Climate variables also play a crucial role in the occurrence of forest fires [47,48]. In this study, the variables of average temperature, average relative humidity, precipitation, and average wind speed were used. The climatological data from 2001 to 2020 for China were acquired from the National Meteorological Information Center (<http://data.cma.cn/>), accessed on 13 August 2021. The climate variables obtained from discrete stations were transformed into surface data using the inverse distance weighting interpolation.

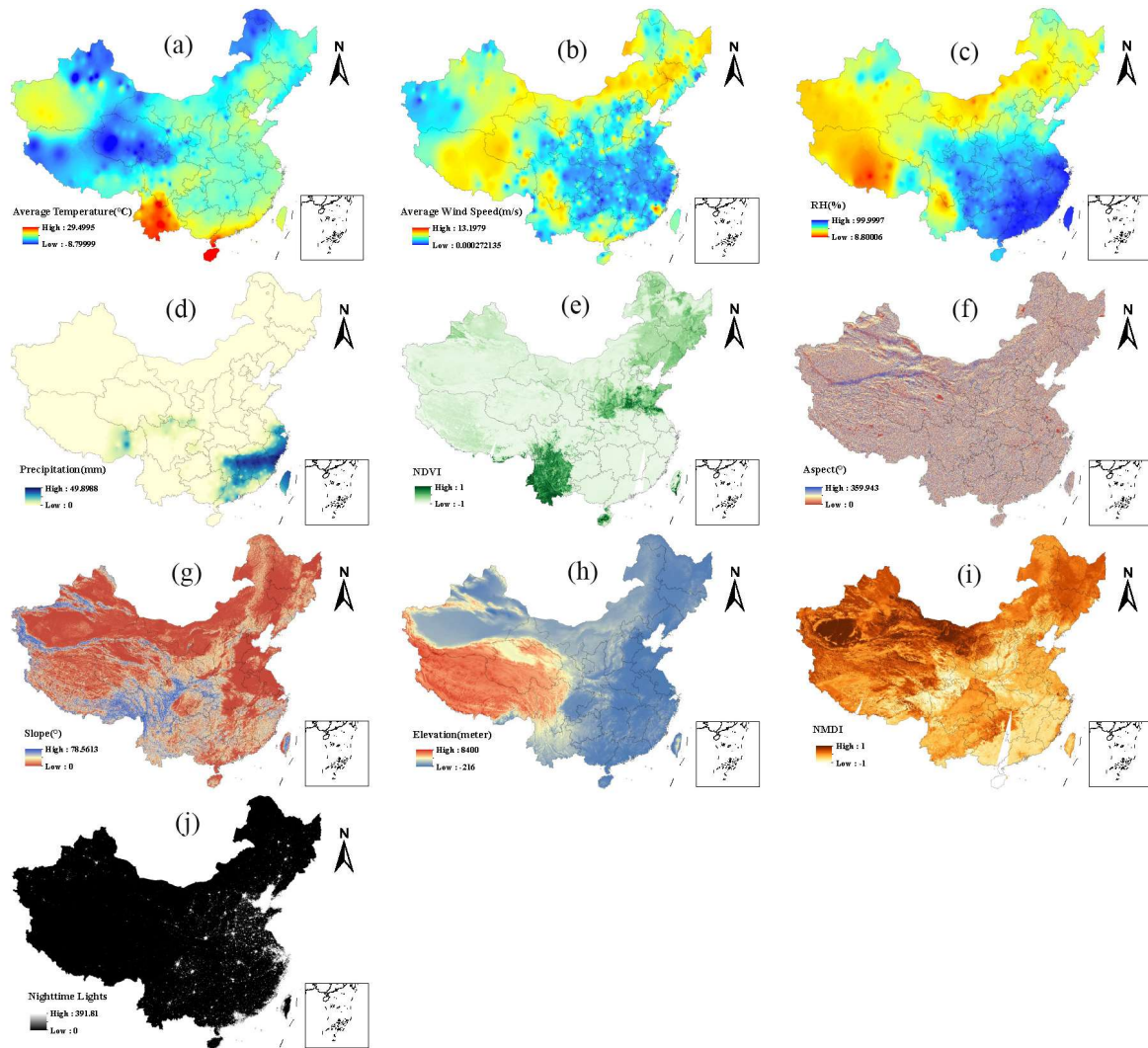


Figure 3. The spatial distribution of variables on 30 May 2020. In (a–j), different values of the spatial distribution of fire risk factors were projected onto the study area.

Combustible variables were chosen to include land cover [49,50], NDVI [51], and NMDI [52]. The land cover data consist of 17 different land cover types with a resolution of 500 m. Specifically, we focused on the first seven land types (evergreen needleleaf, evergreen broadleaf, deciduous needleleaf, deciduous broadleaf, mixed forests, closed shrubland, open shrublands), which represent forest areas. To assess the health and water content of vegetation, NDVI and NMDI were used. NDVI quantifies vegetation by analyzing the disparity between near-infrared and red spectral bands using Equation (1). Additionally, the NMDI was utilized to monitor the moisture content of both soil and vegetation through spatial remote sensing methods using Equation (2).

$$NDVI = \frac{R_{860nm} - R_{645nm}}{R_{860nm} + R_{645nm}} \quad (1)$$

$$NMDI = \frac{R_{860nm} - (R_{1640nm} - R_{2130nm})}{R_{860nm} + (R_{1640nm} + R_{2130nm})} \quad (2)$$

where R is reflectivity of each band and the subscripts correspond to the surface reflectance at the central wavelengths of 645, 860, 1640, and 2130 nm bands in the MODO9GA product.

Typically, fires have a higher chance of occurring near urban forest borders where human activity was more concentrated [53–55]. In this study, we chose to utilize nighttime

light data, which was correlated with social indicators and can easily be processed to show spatialized results [56]. Specifically, annual stable light images from DMSP/OLS for the years 2001–2013 and annual average nighttime light images from VIRRS for the years 2014–2020 were utilized. With these data, the nearest non-zero pixel to the historical fire was located using proximity analysis. Then, the Euclidean distance between the fire and the light was calculated as the nighttime light value.

3. Methodology

3.1. Convolutional Neural Network (CNN)

The convolutional neural network (CNN) was originally proposed to solve the speech recognition problem [57]. With hidden layers, it is able to identify simple patterns within original data, then use these simplified patterns to compute more complex patterns in advanced layers. To be specific, CNN was an input-to-output mapping network, consisting of input, hidden, and output layers [28]. The network was proficient in learning a vast array of mapping relations, despite the lack of a precise mathematical representation of the hidden layer lying between inputs and outputs. Hidden layers include several common types of constructs, such as convolutional layers, pooling layers, and fully connected layers [58]. The convolutional layer automatically extracted features from various regions across the input, performing operations like local sensory field and weight sharing to reduce the memory consumption of the deep network [59]. The pooling layer preserves features while compressing data [60]. The fully connected layer distributes high-level features from the convolutional layer, like a basic classification neural network, resulting in the final output. Furthermore, as a feedforward neural network, CNN ensures that the three operations of local sensory field, weight sharing, and pooling layer work cohesively. They are able to reduce the number of network parameters and preventing overfitting. In this study, we utilized 11 feature functions as the input data. With the aim of predicting forest fire occurrence probability, the output layer produces a binary classification result. Figure 4 illustrates the convolutional neural network architecture. Therefore, a one-dimensional convolutional neural network was employed for our research.

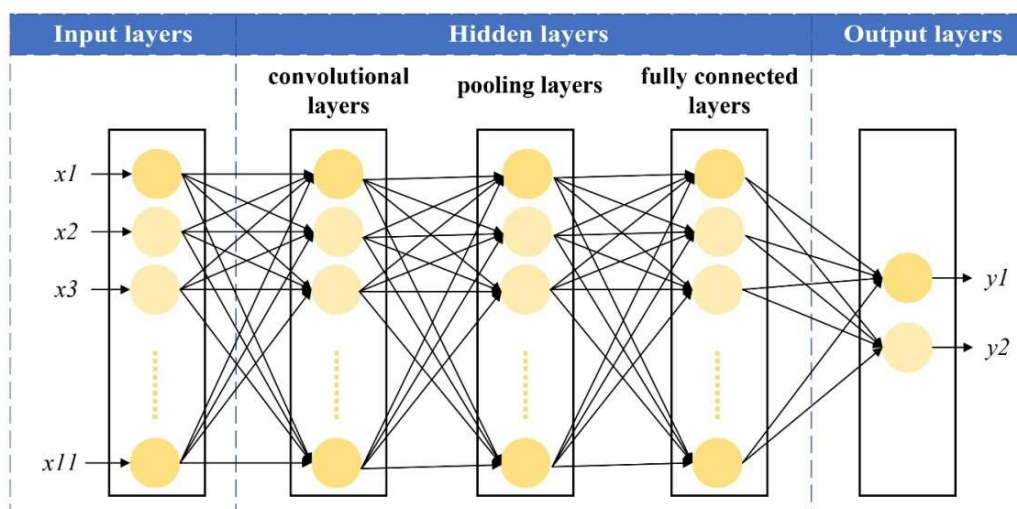


Figure 4. Convolutional neural network architecture. The input layer has 11 feature functions (corresponding to risk factors), the output is the probability result of the binary classification problem. Same color does not mean same object.

3.2. Particle Swarm Optimization (PSO)

Particle swarm optimization (PSO) is an evolutionary computation technique based on group collaboration and random search algorithms [61]. It was developed to simulate the foraging behavior of a flock of birds using massless particles with only velocity and position properties [62,63]. The algorithm has explicit upper and lower limits for each

particle. Each particle individually searches for an optimal solution in the search space and records it as the current personal best value (*pbest*). These particles then share their individual best with other particles in the swarm, and the optimal individual best value is selected as the current global best value (*gbest*) for the entire swarm. Based on the *pbest* and *gbest* values sharing throughout the search space, all particles iteratively update their velocity and position [64]. This is repeated many times until the global extreme value (*Gbest*) is found. The particle updates its velocity and position to find these two optimal values which follows the standard Equations (3) and (4) [65]:

$$V_i^{t+1} = \omega V_i^t + c_1 r_1 (xBest_i^t - x_i^t) + c_2 r_2 (gBest_i^t - x_i^t) \quad (3)$$

$$x_i^{t+1} = x_i^t + V_i^t \cdot t \quad (4)$$

where t refers to number of iterations. V_i^t represents the velocity of the i th particle in t th iteration, and x_i^t is the position of the i th particle in t th iteration. ω , c_1 , c_2 , r_1 , and r_2 are, respectively, inertia weight, two learning rate values, and two random parameters within $[0, 1]$. The introduction of ω tunes the global and local search capability.

3.3. PSO-CNN Method

In the application of CNN, the main challenge was selecting its architecture and parameters. Empirical parameters often only apply to specific research data and have limited generalization. To optimize CNN, a novel approach has been developed, which uses the random but guided mode of the PSO algorithm to evolve both the architecture and parameters of the CNN. By training the dataset in the designated search space, parameters were effectively optimized. In addition, human intervention was required to determine the search space.

The optimization principle of the methodology was using the configuration of CNN as the particle of the PSO. Each particle iteratively obtains the configuration of CNN with the best accuracy. During the training of the PSO-CNN, the CNN extracted features from training data and calculated the classification probability in its final Softmax layer, corresponding to the probability of fire occurrence. The accuracy obtained corresponds to the fitness value of each particle. The specific flowchart of PSO-CNN is shown (see Figure 5).

Step 1: In the data pre-processing, based on the dimensionality requirements of one-dimensional CNN, we binarized and incremented the dimensionality of the dataset.

Step 2: Initialize and generate CNN architecture as particles of PSO. The training run times m_max of CNN is 4 and epoch is 100. The particle number and the iteration number of PSO is 5.

Step 3: Train and iterate each initialization particle to obtain *Gbest*, and the CNN model S_i corresponding to *Gbest* is the best model before optimization.

Step 4: Employ PSO to optimize the architecture parameters, then update the position and architecture of each particle in turn. Equation (5) is used to evaluate the fitness and loss value of each particle in each iteration. When the fitness value A_i is greater than the value of the last iteration A_{i-1} , it would update the *pbest* of each particle. When *pbest* is greater than the current *gbest* value, update the *gbest* value until the global extreme value (*Gbest*) is obtained.

$$fitness = \frac{1}{N} \sum |t(i) - y(i)| \quad (5)$$

where N refers to the number of samples in the training data; $t(i)$ and $y(i)$, respectively, refer to the actual and predicted data.

Step 5: Finally, *Gbest* is obtained, and the evolved model will be trained for 100 epochs, so that it can improve the fitness value.

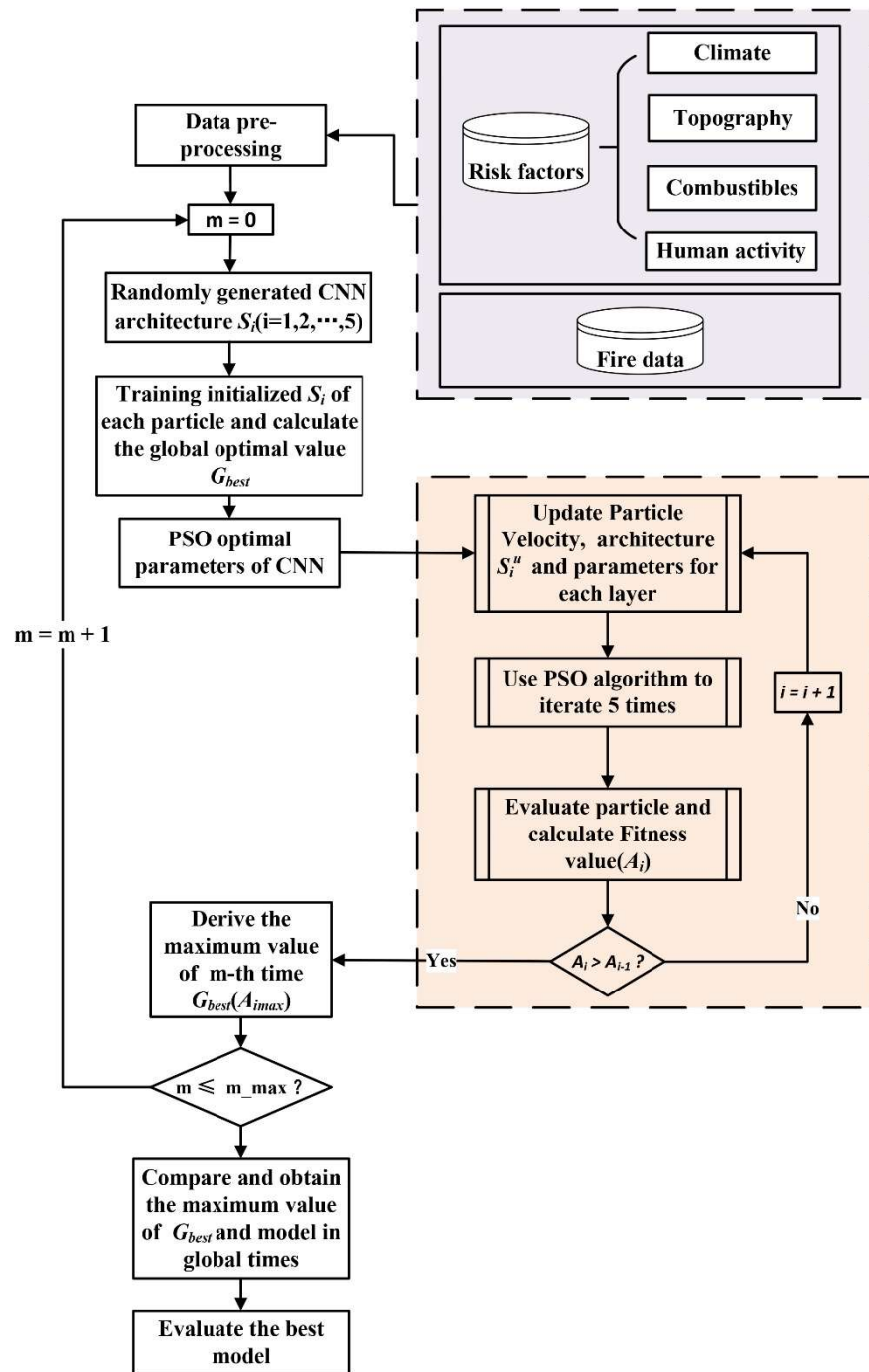


Figure 5. The flowchart represents how this model works. The blue box indicates the data part. The yellow box shows the PSO optimization search process. S_i in the figure is the structure of each CNN, and the subscripted i is the particle. G_{best} is the global extreme value. A_i is the fitness value.

To ensure a balanced distribution and avoid an excessive number of similar samples after splitting, we utilized the `train_test_split` function with the shuffling option set to True and a fixed `random_state` value [66–68]. For the fire probabilities obtained from the test group (30%). We spatially visualized them as a national fire risk map. To be specific, the forest fire probability is classified into five levels risk: very low (0–0.2), low (0.2–0.4), medium (0.4–0.6), high (0.6–0.8), and very high (0.8–1).

3.4. Evaluation Metrics

In order to get details about the impact of different risk factor on the model prediction [67], we used shapely values (SHAP) to quantitatively evaluate the contribution of the input factors to the prediction of PSO-CNN model. For this technique, the core idea is to compute the marginal contribution of features to the model output, which is widely used in the literature [67].

In this study, the proposed model was evaluated using accuracy (the correct prediction rate) and ROC (receiver operating characteristic curve) for our dataset [13]. The ROC was plotted with dichotomous coordinates, and the model's accuracy was determined by the AUC (area under the curve) [69]. Typically, a model that has an AUC greater than 0.9 was considered to fit extremely well [70]. Additionally, the performance of PSO-CNN model could be compared with that of other models such as logistic regression (LR) [69,71,72], random forest (RF) [72,73], support vector machine (SVM) [17,74], k-nearest neighbor (KNN) [75], and CNN.

4. Results

4.1. The Architecture of Optimized CNN Using PSO

As depicted in Figure 6, the architectural configuration of the best model was derived from five independent runs. The model comprised a well-organized six-layer structure. The initial three layers were convolutional layers, followed by one pooling and one fully connected layer, and finally another convolutional layer. This structural distribution showed the best training results. This model, as presented in Table 2, consists of a total of 687,280 parameters. Notably, 685,320 parameters have already been trained, accounting for 99.7% of all parameters. Only a mere 1960 parameters remain untrained.

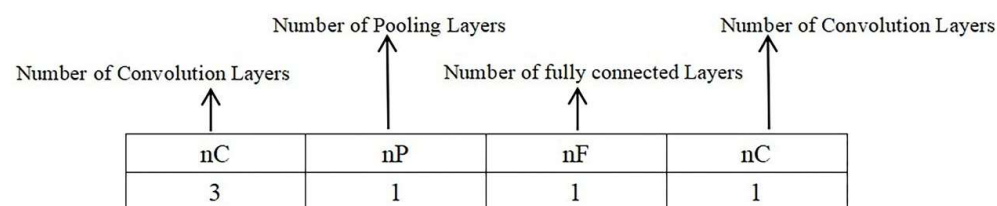


Figure 6. Architecture of the optimized model. Order of the layers obtained from left to right.

Table 2. The table represents the parameters of the CNN structure that were trained by the PSO as well as the parameters that were not trained.

Total Parameters	Trainable Parameters	Non-Trainable Parameters
687,280	685,320	1960

4.2. The Performance of Traditional CNN and Optimized CNN

Based on Section 4.1, the comparison of results obtained from PSO-CNN models and CNN was shown as Figure 7. The conventional CNN model achieved accuracy rates of 79.66% at its peak and 77.11% at its lowest point. On the other hand, the PSO-optimized CNN model demonstrated higher levels of accuracy, with a maximum rate of 83.73% and a minimum rate of 82.92%. During the same run time, the disparity in accuracy between these two models reached a maximum of 6%, with a minimum of over 4%. Furthermore, the optimized model consistently maintained an accuracy of approximately 83%.

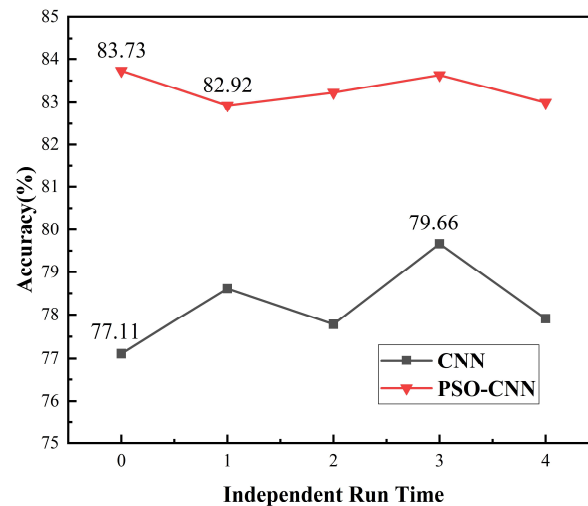


Figure 7. Comparison of results obtained from PSO-CNN and CNN. Independent run time corresponds to m in Figure 5. The red dash is the accuracy of the PSO-CNN. The black dash is the accuracy of the CNN.

4.3. Impact of Risk Factors on Model Prediction

SHAP technique allows for global or local interpretation of model prediction. In this study, only the summary_plot method was used to find the importance of risk factors for PSO-CNN model. This result (Figure 8) showed that NDVI and land cover have the highest contribution to the predictions of this model. These results are reasonably consistent with results reported in the literature [76].

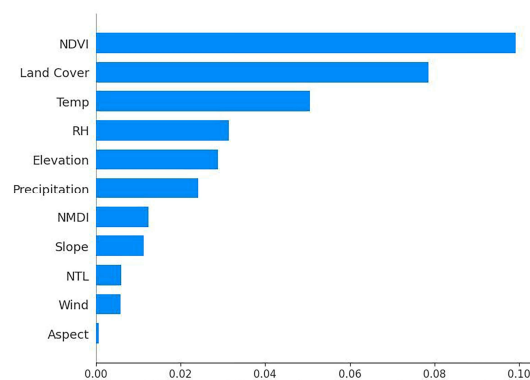


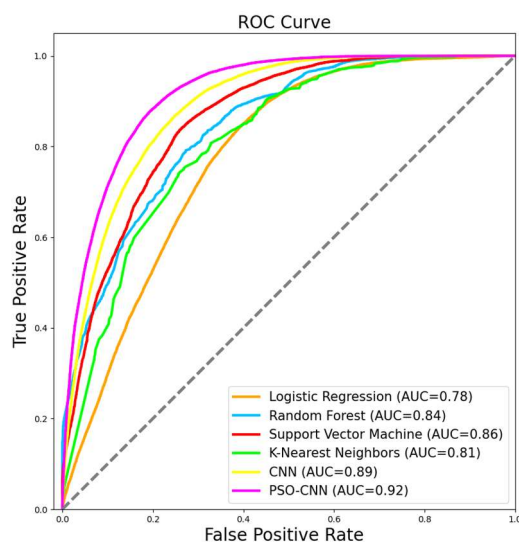
Figure 8. The importance of risk factors for PSO-CNN model. The x-axis represents the average of each variable's absolute SHAP value, with variables ranked vertically based on their impact. The y-axis represents the input risk factors in this study.

4.4. Accuracy Comparison of Different Models

We evaluated the performance of the proposed model against other models trained using the same training group. As presented in Table 3, the PSO-CNN model demonstrated a prediction accuracy of 82.2%, exceeding RF by approximately 9%, LR by about 11%, SVM by about 8%, and KNN by about 11%. The ROC curves of these models, as shown in Figure 9, demonstrated that PSO-CNN exhibits the highest AUC of 0.92. Our analysis suggested that PSO-CNN was the best prediction model among CNN, LR, RF, SVM, and KNN, with an AUC of 0.89, 0.82, 0.84, 0.86, and 0.81, respectively. Moreover, PSO-CNN improved AUC performance by about 4% compared to CNN.

Table 3. Comparison of training and testing accuracies of the six models.

Models	Accuracy	
	Training	Validation
Logistic Regression	73.0	71.5
Random Forest	74.5	72.9
Support Vector Machine	75.5	74.7
K-Nearest Neighbor	72.6	70.9
CNN	79.6	77.4
PSO-CNN	83.7	82.2

**Figure 9.** ROC curves comparison for the six models. The area under each curve represents the AUC value. the AUC is defined as a value from 0 to 1.

4.5. Spatial Distribution of Different Models

Figure 10 presented the percentages of each model's risk level on 30 May 2020, for selected data based on their prediction results. The proposed model's risk levels were interpolated into a forest fire risk distribution map utilizing the Kriging method from ArcGIS 10.8 software, utilizing forest cover data from 2020. The PSO-CNN model has the highest prediction rate (57.1%) for very high risk fires, while the other three models have only 11.8%, 3.8%, and 0, respectively. This suggests that the proposed model can improve the effectiveness of forest fire protection in real situations.

Figure 11 assessed the distribution of fire on 30 May 2020, accompanied by a predicted fire risk distribution area and local zoom-in maps of fire. In particular, compared to the other models' predictions of medium-low risk, the PSO-CNN model predicted the Xiaoxing'an Mountain region and the Liangshan region of Sichuan as medium-high risk areas. In addition, it was possible to visualize the fire risk level of the image element units through the local zoomed-in map of fires in northern Yunnan, and there were variations in the prediction results of different models for the same fire. For instance, the PSO-CNN model predicted a very high risk, while the other four models predicted medium risk, and the traditional CNN results indicated high risk. Overall, the PSO-CNN model demonstrated a remarkable level of accuracy and detail in dividing forest fire areas, highlighting its high practical potential.

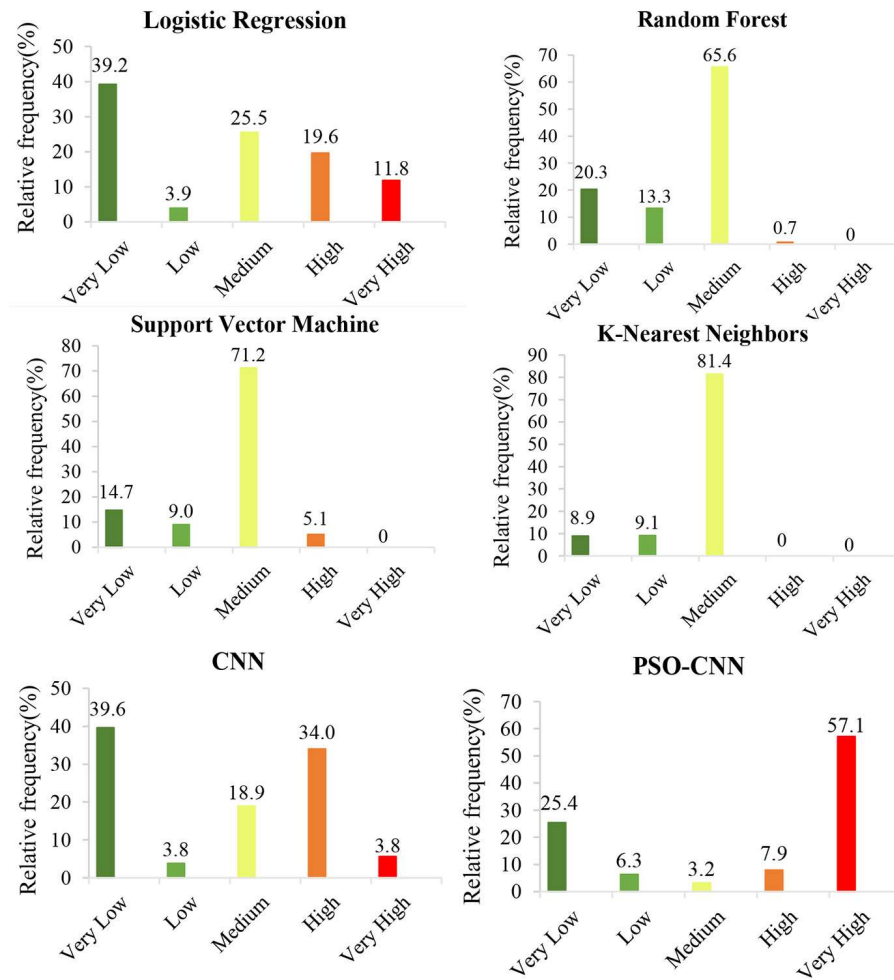


Figure 10. Proportion of each risk class predicted by the four models. The dark green bars are very low risk, the light green bars are low risk, and the yellow bars are medium risk, and the orange bars are high risk and the red bars are very high risk.

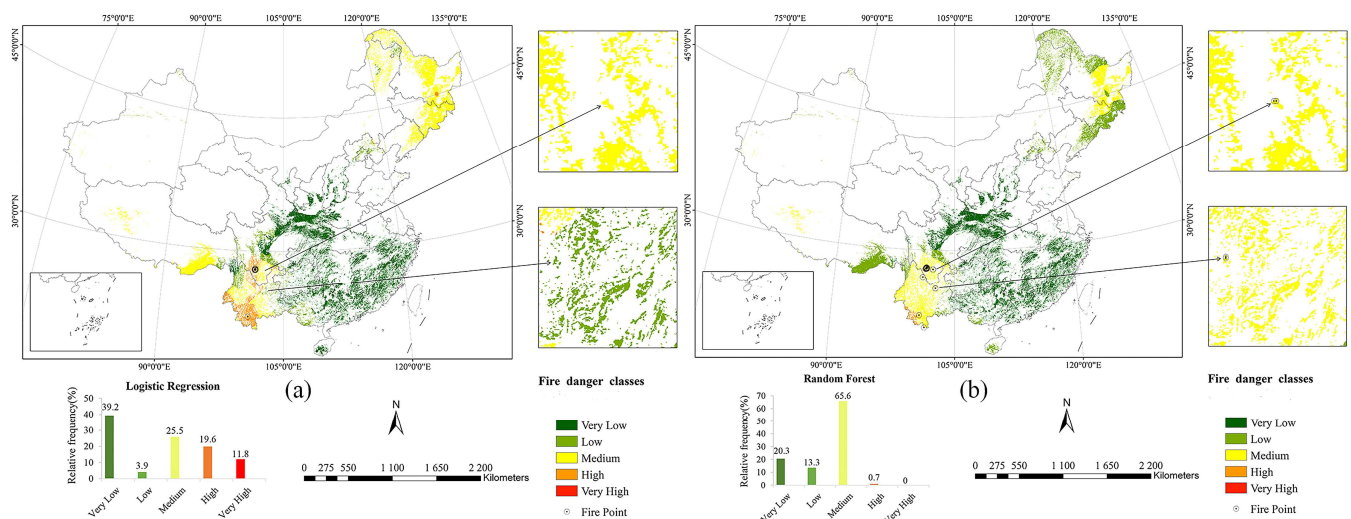


Figure 11. Cont.

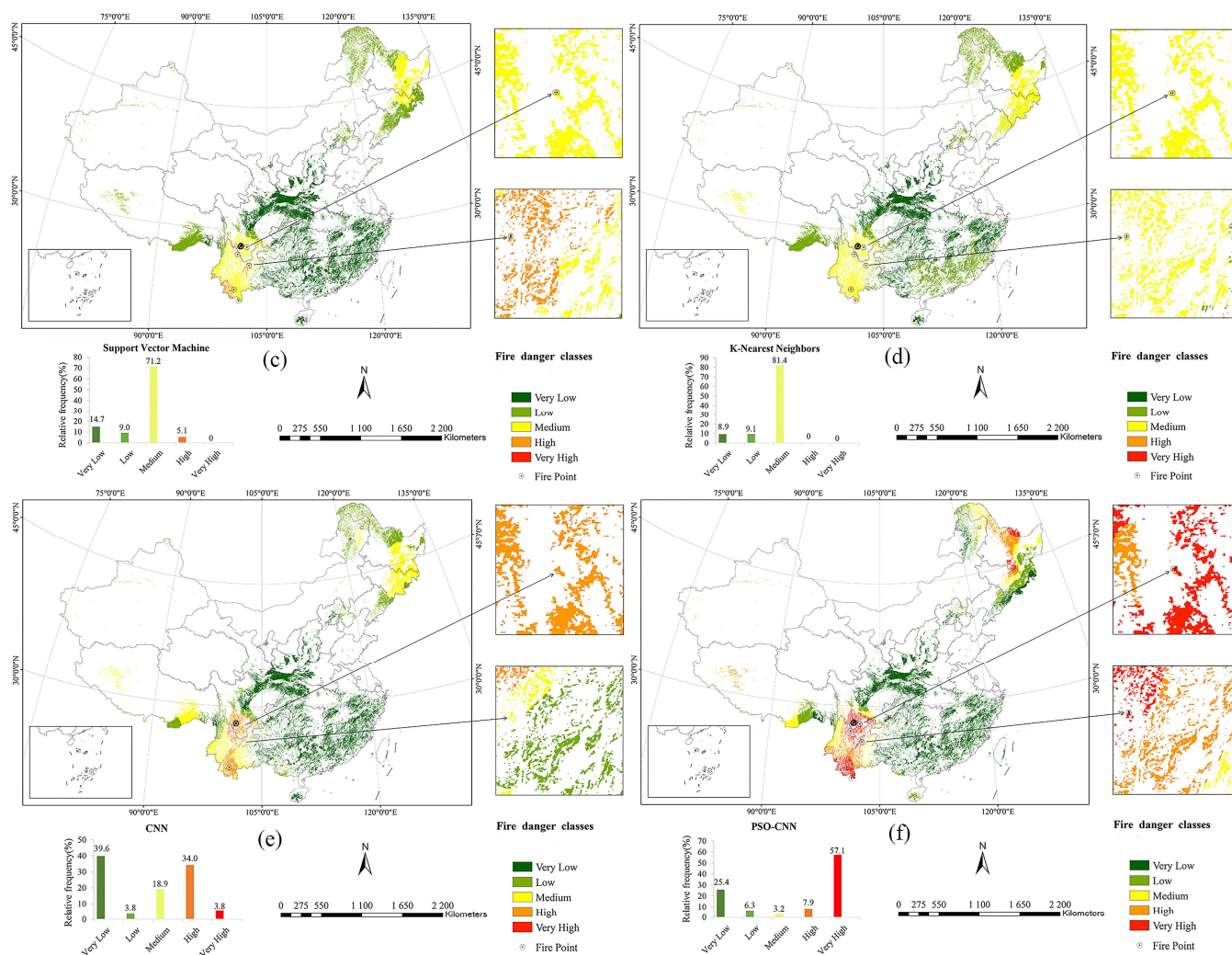


Figure 11. Spatial distribution of forest fire risk in China according to different models. In (a–f), the large figure on the left shows the results of the risk level distribution predicted by each of the six different models. The meanings represented by the colors are shown in Figure 10. The two small figures on the right are local zoomed-in images of different places, and the area where the fire falls indicates that it is predicted to be of the corresponding risk level. The starting point of the arrow is the location of the specific fire.

5. Discussion

5.1. Results Discussion

Forest fires generally exhibit non-linear relationships with various risk factors [77]. To effectively quantify this non-linear relationship, advanced deep learning models (e.g., CNN) are suitable [22]. In previous research conducted within this study area, the accuracy values obtained are on average 73% [40], 80% [73], and 82% [41], respectively. In this study, the proposed PSO-CNN model exhibited superior performance (training accuracy = 83.7%, validation accuracy = 82.2%).

A conventional CNN model was developed in this study and the network parameters were trained using Adam’s optimizer. However, the outcomes obtained were not up to the desired level of satisfaction. Consequently, we suggested employing a more efficient optimization technique (i.e., PSO) [29]. Compared to other swarm intelligence (SI) algorithms for optimization problems, PSO and ant colony optimization (ACO) performed well [78]. According to Mavrovouniotis et al. [79], PSO was more effective than other evolutionary methods like differential evolution (DE) and genetic algorithm (GA) in optimizing the network and parameters. Therefore, PSO is an outstanding optimization tool. Previous

research has successfully used PSO to optimize neural networks in various applications, such as adaptive improved PSO-based RBF (AI-PSO-RBF) [80], nonlinear-time-varying evolutionary PSO (NTVE-PSO) [81], particle swarm optimization-sliding mode control (PSO-SMC) [82], and multi-objective particle swarm optimization algorithm with competitive mechanism (MOPSO-CM) [83], and so on. These studies also demonstrated the effectiveness of PSO as an optimization tool.

The optimal configurations of the proposed model were automatically determined within a given search space. Specifically, PSO deployed particle velocity and position updates to identify optimal parameters. The results obtained from this research demonstrated that optimization performance was influenced by the number of particles and epochs. It was possible to deduce that increasing these two parameters could generate a more efficient CNN architectures. However, this process would consume more computational memory and time. Therefore, finding a middle ground between accurate predictions and efficient computation was crucial. Even though deep learning is more computationally complex than machine learning, it was more adaptable and better suited to handling nonlinear problems, particularly in the context of large datasets. As the most popular CNN in deep learning, its 1D CNNs offered excellent training performance while retaining low computational complexity in many applications [84,85]. Additionally, deep learning architecture was prone to instability due to minor data or parameter changes [86]. However, the PSO-CNN model's prediction stability, demonstrated by its consistently smooth results in five consecutive independent runs averaging approximately 83%. This demonstrated the potential for stability development.

In order to validate the effectiveness of the model, we established used forest fire prediction models, such as LR [12,13,71], RF [14,17], SVM [17,74], and KNN [75]. The PSO-CNN model outperformed the other three models, including CNN. It was hypothesized that the reason may lie in the former's insufficient ability to train and extract information from multi-source and non-linear data [17], but our proposed method was better able to take full advantage of its strengths in dealing with such problems. Moreover, the PSO-CNN model demonstrated a higher prediction rate for very high risk levels, indicating its heightened sensitivity to risk factors. Due to the large forest cover and high vulnerability to climate extremes, the southwest and northeast regions are particularly prone to higher fire risk. Consequently, these regions were prioritized for fire prevention and management efforts, ensuring the efficient allocation of management resources.

While other risk factors associated with human activity are frequently used in predicting wildfire risk, nighttime light is not routinely considered. However, the presence of nighttime lights was frequently linked to public safety [87]. Some research studies also have demonstrated the usefulness of nighttime lights in pollution disaster assessment [88] and armed conflict monitoring [89]. To accurately characterize human activity, this research computed the proximity between lights and fire. This key operation helped to eliminate the nighttime lights data of non-forested areas and ensures the accurate characterization of the data. Importantly, most of the human activity indicators often used, such as distance from roads and distance from settlements [90], are usually static and do not change rapidly. However, human activity is not constant. Therefore, nighttime lights are able to respond to the degree of social prosperity [91], which is consistent with the dynamic nature of human activities. Therefore, nighttime lights are useful for perfecting data on forest fire risk factors.

5.2. Improvement Strategies

Although this study has provided valuable insights, it is essential to recognize certain limitations. Firstly, due to the broad research area and limited daily data, spatial interpolation may produce imprecise predictions in some regions, and this may reduce the overall accuracy. In addition, we have encountered certain issues with risk factors selection process, such as the absence of thunderstorm activity data and restrictions of the nighttime light in expressing human activity (e.g., railways characterized by weak lighting). Similarly, the interpretability of the impact factors in the black box has not been considered in this

paper. In future, we are committed to enhancing our factor selection and research of impact mechanisms to address these challenges effectively.

Moreover, there was a strong correlation between forest fire incidence and geographic distribution, but this study did not take into account the spatial heterogeneity of fire locations or utilize relevant spatial information. To solve these limitations, future research could integrate spatial heterogeneity with deep learning, so that a combined prediction model can be built.

6. Conclusions

To address the exploration of optimization algorithms in deep learning, we used particle swarm optimization algorithms to optimize CNN. Without much human intervention, the process of searching for the CNN's configuration in a certain search space is automated. Based on the forest fire data of mainland China from 2001 to 2020, including 11 forest fire risk factors (such as meteorology, topography, combustibles, and human activities), we used the obtained PSO-CNN model for forest fire risk prediction. The prediction accuracy of this model was compared with logistic regression, random forest, support vector machine, k-nearest neighbor, and CNN. The following conclusions were drawn:

- (1) The established conventional CNN model can be utilized for forest fire prediction, and it exhibits greater potential.
- (2) The optimized CNN of PSO algorithm outperformed the traditional CNN in prediction, representing a novel approach in the realm of forest fire research.
- (3) Through testing and comparison with other models (such as logistic regression, random forest, support vector machine and k-nearest neighbor), it has been determined that the different evaluation metrics (accuracy, ROC) demonstrate superior performance. Furthermore, when mapping the fire risk in the study area, there is a heightened sensitivity to fire risk.

In summary, this PSO-CNN model can effectively predict the occurrence of forest fires. It plays a positive leading role in the research of forest fire prediction based on evolutionary deep learning.

Author Contributions: Conceptualization, J.L. and Z.Z.; methodology, X.Y. and Z.Z.; software, X.Y. and J.C.; validation, X.Y. and S.G.; formal analysis, K.Y., X.Y. and X.L.; investigation, X.Y.; resources, L.Y.; data curation, K.Y.; writing—original draft preparation, X.Y.; writing—review and editing, X.Y. and Z.Z. and L.Y.; visualization, X.Y. and Z.Z.; supervision, Z.Z. and K.Y.; project administration, Z.Z.; funding acquisition, Z.Z. and K.Y. All authors have read and agreed to the published version of the manuscript.

Funding: This research was funded by the National Natural Science Foundation of China, grant number 41801315.

Data Availability Statement: The data presented in this study are available upon request from the corresponding author.

Acknowledgments: We would like to thank the editor and anonymous reviewers for their thoughtful and helpful comments.

Conflicts of Interest: The authors declare no conflicts of interest.

References

1. Bowman, D.M.; Balch, J.K.; Artaxo, P.; Bond, W.J.; Carlson, J.M.; Cochrane, M.A.; D'Antonio, C.M.; Defries, R.S.; Doyle, J.C.; Harrison, S.P.; et al. Fire in the Earth system. *Science* **2009**, *324*, 481–484. [[CrossRef](#)] [[PubMed](#)]
2. Archibald, S.; Lehmann, C.E.R.; Belcher, C.M.; Bond, W.J.; Bradstock, R.A.; Daniau, A.L.; Dexter, K.G.; Forrester, E.J.; Greve, M.; He, T.; et al. Biological and geophysical feedbacks with fire in the Earth system. *Environ. Res. Lett.* **2018**, *13*, 033003. [[CrossRef](#)]
3. Scott, A.C.; Glasspool, I.J. The diversification of Paleozoic fire systems and fluctuations in atmospheric oxygen concentration. *Proc. Natl. Acad. Sci. USA* **2006**, *103*, 10861–10865. [[CrossRef](#)] [[PubMed](#)]
4. Zheng, Z.; Gao, Y.; Zhang, J.; Chen, Z. Modeling the susceptibility of forest fires using a genetic algorithm: A case study in mountain areas of southwestern China. *Sci. Program.* **2022**, *2022*, 5502209. [[CrossRef](#)]

5. Li, W.; Xu, Q.; Yi, J.-h.; Liu, J. Predictive model of spatial scale of forest fire driving factors: A case study of Yunnan Province, China. *Sci. Rep.* **2022**, *12*, 19029. [[CrossRef](#)] [[PubMed](#)]
6. Lv, C.; Wang, J.; Zhang, F. Forest fire spread model based on the grey system theory. *J. Supercomput.* **2018**, *76*, 3602–3614. [[CrossRef](#)]
7. Zheng, Z.; Huang, W.; Li, S.; Zeng, Y. Forest fire spread simulating model using cellular automaton with extreme learning machine. *Ecol. Modell.* **2017**, *348*, 33–43. [[CrossRef](#)]
8. Zheng, Z.; Zeng, Y.; Li, S.; Huang, W. Mapping burn severity of forest fires in small sample size scenarios. *Forests* **2018**, *9*, 608. [[CrossRef](#)]
9. Zheng, Z.; Zeng, Y.; Li, S.; Huang, W. A new burn severity index based on land surface temperature and enhanced vegetation index. *Int. J. Appl. Earth Obs. Geoinf.* **2016**, *45*, 84–94. [[CrossRef](#)]
10. Archibald, S.; Lehmann, C.E.; Gomez-Dans, J.L.; Bradstock, R.A. Defining pyromes and global syndromes of fire regimes. *Proc. Natl. Acad. Sci. USA* **2013**, *110*, 6442–6447. [[CrossRef](#)]
11. Ye, J.; Wu, M.; Deng, Z.; Xu, S.; Zhou, R.; Clarke, K.C. Modeling the spatial patterns of human wildfire ignition in Yunnan province, China. *Appl. Geogr.* **2017**, *89*, 150–162. [[CrossRef](#)]
12. Lozano, F.J.; Suárez-Seoane, S.; de Luis, E. Assessment of several spectral indices derived from multi-temporal Landsat data for fire occurrence probability modelling. *Remote Sens. Environ.* **2007**, *107*, 533–544. [[CrossRef](#)]
13. Catry, F.X.; Rego, F.C.; Bação, F.L.; Moreira, F. Modeling and mapping wildfire ignition risk in Portugal. *Int. J. Wildland Fire* **2009**, *18*, 921–931. [[CrossRef](#)]
14. Wu, Z.; He, H.S.; Yang, J.; Liu, Z.; Liang, Y. Relative effects of climatic and local factors on fire occurrence in boreal forest landscapes of northeastern China. *Sci. Total Environ.* **2014**, *493*, 472–480. [[CrossRef](#)] [[PubMed](#)]
15. Rodrigues, M.; de la Riva, J.; Fotheringham, S. Modeling the spatial variation of the explanatory factors of human-caused wildfires in Spain using geographically weighted logistic regression. *Appl. Geogr.* **2014**, *48*, 52–63. [[CrossRef](#)]
16. Tien Bui, D.; Bui, Q.-T.; Nguyen, Q.-P.; Pradhan, B.; Nampak, H.; Trinh, P.T. A hybrid artificial intelligence approach using GIS-based neural-fuzzy inference system and particle swarm optimization for forest fire susceptibility modeling at a tropical area. *Agric. For. Meteorol.* **2017**, *233*, 32–44. [[CrossRef](#)]
17. Ngoc Thach, N.; Bao-Toan Ngo, D.; Xuan-Canh, P.; Hong-Thi, N.; Hang Thi, B.; Nhat-Duc, H.; Dieu, T.B. Spatial pattern assessment of tropical forest fire danger at Thuan Chau area (Vietnam) using GIS-based advanced machine learning algorithms: A comparative study. *Ecol. Inform.* **2018**, *46*, 74–85. [[CrossRef](#)]
18. Sevinc, V. Mapping the forest fire risk zones using artificial intelligence with risk factors data. *Environ. Sci. Pollut. Res.* **2023**, *30*, 4721–4732. [[CrossRef](#)]
19. Zheng, Z.; Gao, Y.; Yang, Q.; Zou, B.; Xu, Y.; Chen, Y.; Yang, S.; Wang, Y.; Wang, Z. Predicting forest fire risk based on mining rules with ant-miner algorithm in cloud-rich areas. *Ecol. Indic.* **2020**, *118*, 106772. [[CrossRef](#)]
20. Şatır, O.; Berberoglu, S.; Donmez, C. Mapping regional forest fire probability using artificial neural network model in a Mediterranean forest ecosystem. *Geomat. Nat. Hazards Risk* **2016**, *7*, 1645–1658. [[CrossRef](#)]
21. Zhang, C.; Pan, X.; Li, H.; Gardiner, A.; Sargent, I.; Hare, J.; Atkinson, P.M. A hybrid MLP-CNN classifier for very fine resolution remotely sensed image classification. *ISPRS J. Photogramm. Remote Sens.* **2018**, *140*, 133–144. [[CrossRef](#)]
22. Zhang, G.; Wang, M.; Liu, K. Forest fire susceptibility modeling using a convolutional neural network for Yunnan Province of China. *Int. J. Disaster Risk Sci.* **2019**, *10*, 386–403. [[CrossRef](#)]
23. Nguyen, H.D. Hybrid models based on deep learning neural network and optimization algorithms for the spatial prediction of tropical forest fire susceptibility in Nghe An province, Vietnam. *Geocarto Int.* **2022**, *37*, 11281–11305. [[CrossRef](#)]
24. Reis, H.C.; Turk, V. Detection of forest fire using deep convolutional neural networks with transfer learning approach. *Appl. Soft Comput.* **2023**, *143*, 110362. [[CrossRef](#)]
25. Huang, L.; Liu, G.; Wang, Y.; Yuan, H.; Chen, T. Fire detection in video surveillances using convolutional neural networks and wavelet transform. *Eng. Appl. Artif. Intell.* **2022**, *110*, 104737. [[CrossRef](#)]
26. Ban, Y.; Zhang, P.; Nascetti, A.; Bevington, A.R.; Wulder, M.A. Near Real-Time Wildfire Progression Monitoring with Sentinel-1 SAR Time Series and Deep Learning. *Sci. Rep.* **2020**, *10*, 1322. [[CrossRef](#)]
27. Zhao, W.; Du, S.; Emery, W.J. Object-based convolutional neural network for high-resolution imagery classification. *IEEE J. Sel. Top. Appl. Earth Obs. Remote Sens.* **2017**, *10*, 3386–3396. [[CrossRef](#)]
28. Barzegar, R.; Aalami, M.T.; Adamowski, J. Short-term water quality variable prediction using a hybrid CNN–LSTM deep learning model. *Stoch. Environ. Res. Risk Assess.* **2020**, *34*, 415–433. [[CrossRef](#)]
29. Singh, P.; Chaudhury, S.; Panigrahi, B.K. Hybrid MPSO-CNN: Multi-level Particle Swarm optimized hyperparameters of Convolutional Neural Network. *Swarm Evol. Comput.* **2021**, *63*, 100863. [[CrossRef](#)]
30. Tian, D.; Shi, Z. MPSO: Modified particle swarm optimization and its applications. *Swarm Evol. Comput.* **2018**, *41*, 49–68. [[CrossRef](#)]
31. Fang, K.; Yao, Q.; Guo, Z.; Zheng, B.; Du, J.; Qi, F.; Yan, P.; Li, J.; Ou, T.; Liu, J.; et al. ENSO modulates wildfire activity in China. *Nat. Commun.* **2021**, *12*, 1764. [[CrossRef](#)] [[PubMed](#)]
32. Ying, L.; Han, J.; Du, Y.; Shen, Z. Forest fire characteristics in China: Spatial patterns and determinants with thresholds. *For. Ecol. Manag.* **2018**, *424*, 345–354. [[CrossRef](#)]
33. Fang, L.; Yang, J.; Zu, J.; Li, G.; Zhang, J. Quantifying influences and relative importance of fire weather, topography, and vegetation on fire size and fire severity in a Chinese boreal forest landscape. *For. Ecol. Manag.* **2015**, *356*, 2–12. [[CrossRef](#)]
34. Giglio, L.; Schroeder, W.; Justice, C.O. The collection 6 MODIS active fire detection algorithm and fire products. *Remote Sens. Environ.* **2016**, *178*, 31–41. [[CrossRef](#)] [[PubMed](#)]

35. Giglio, L.; Descloitres, J.; Justice, C.O.; Kaufman, Y.J. An enhanced contextual fire detection algorithm for MODIS. *Remote Sens. Environ.* **2003**, *87*, 273–282. [[CrossRef](#)]
36. Tian, X.; Shu, L.; Wang, M.; Zhao, F.; Chen, L. The fire danger and fire regime for the Daxing'anling Region for 1987–2010. *Procedia Eng.* **2013**, *62*, 1023–1031. [[CrossRef](#)]
37. Adab, H. Landfire hazard assessment in the Caspian Hyrcanian forest ecoregion with the long-term MODIS active fire data. *Nat. Hazards* **2017**, *87*, 1807–1825. [[CrossRef](#)]
38. Chen, D.; Pereira, J.M.C.; Masiero, A.; Pirotti, F. Mapping fire regimes in China using MODIS active fire and burned area data. *Appl. Geogr.* **2017**, *85*, 14–26. [[CrossRef](#)]
39. Radočaj, D.; Jurišić, M.; Gašparović, M. A wildfire growth prediction and evaluation approach using Landsat and MODIS data. *J. Environ. Manag.* **2022**, *304*, 114351. [[CrossRef](#)]
40. Guo, F.; Su, Z.; Wang, G.; Sun, L.; Tigabu, M.; Yang, X.; Hu, H. Understanding fire drivers and relative impacts in different Chinese forest ecosystems. *Sci. Total Environ.* **2017**, *605–606*, 411–425. [[CrossRef](#)]
41. Pang, Y.; Li, Y.; Feng, Z.; Feng, Z.; Zhao, Z.; Chen, S.; Zhang, H. Forest fire occurrence prediction in China based on machine learning methods. *Remote Sens.* **2022**, *14*, 5546. [[CrossRef](#)]
42. Xu, Q.; Li, W.; Liu, J.; Wang, X. A geographical similarity-based sampling method of non-fire point data for spatial prediction of forest fires. *For. Ecosyst.* **2023**, *10*, 100104. [[CrossRef](#)]
43. Jing, X.; Zhang, D.; Li, X.; Zhang, W.; Zhang, Z. Prediction of forest fire occurrence in southwestern China. *Forests* **2023**, *14*, 1797. [[CrossRef](#)]
44. Ge, X.; Yang, Y.; Peng, L.; Chen, L.; Li, W.; Zhang, W.; Chen, J. Spatio-temporal knowledge graph based forest fire prediction with multi source heterogeneous data. *Remote Sens.* **2022**, *14*, 3496. [[CrossRef](#)]
45. Chou, Y.H.; Minnich, R.A.; Chase, R.A. Mapping probability of fire occurrence in San Jacinto Mountains, California, USA. *Environ. Manag.* **1993**, *17*, 129–140. [[CrossRef](#)]
46. Cao, Y.; Wang, M.; Liu, K. Wildfire susceptibility assessment in southern China: A comparison of multiple methods. *Int. J. Disaster Risk Sci.* **2017**, *8*, 164–181. [[CrossRef](#)]
47. Hessel, A.E. Pathways for climate change effects on fire: Models, data, and uncertainties. *Prog. Phys. Geogr.* **2011**, *35*, 393–407. [[CrossRef](#)]
48. Dahan, K.S.; Kasei, R.A.; Hussein, R.; Said, M.Y.; Rahman, M.M. Towards understanding the environmental and climatic changes and its contribution to the spread of wildfires in Ghana using remote sensing tools and machine learning (Google Earth Engine). *Int. J. Digit. Earth.* **2023**, *16*, 1300–1331. [[CrossRef](#)]
49. Oliveira, S.; Moreira, F.; Boca, R.; San-Miguel-Ayán, J.; Pereira, J.M.C. Assessment of fire selectivity in relation to land cover and topography: A comparison between Southern European countries. *Int. J. Wildland Fire* **2014**, *23*, 620–630. [[CrossRef](#)]
50. Carmo, M.; Moreira, F.; Casimiro, P.; Vaz, P. Land use and topography influences on wildfire occurrence in northern Portugal. *Landsc. Urban Plan.* **2011**, *100*, 169–176. [[CrossRef](#)]
51. Chuvieco, E.; Cocero, D.; Riaño, D.; Martín, P.; Martínez-Vega, J.; de la Riva, J.; Pérez, F. Combining NDVI and surface temperature for the estimation of live fuel moisture content in forest fire danger rating. *Remote Sens. Environ.* **2004**, *92*, 322–331. [[CrossRef](#)]
52. Wang, L.; Qu, J.J.; Hao, X. Forest fire detection using the normalized multi-band drought index (NMDI) with satellite measurements. *Agric. For. Meteorol.* **2008**, *148*, 1767–1776. [[CrossRef](#)]
53. Pozzi, F.; Small, C.; Yetman, G. Modeling the distribution of human population with nighttime satellite imagery and gridded population of the world. *Earth Obs. Mag.* **2003**, *12*, 24–30.
54. Archila Bustos, M.F.; Hall, O.; Andersson, M. Nighttime lights and population changes in Europe 1992–2012. *Ambio* **2015**, *44*, 653–665. [[CrossRef](#)] [[PubMed](#)]
55. Hall, O.; Bustos, M.F.A.; Olen, N.B.; Niedomysl, T. Population centroids of the world administrative units from nighttime lights 1992–2013. *Sci. Data* **2019**, *6*, 235. [[CrossRef](#)] [[PubMed](#)]
56. Bagan, H.; Yamagata, Y. Analysis of urban growth and estimating population density using satellite images of nighttime lights and land-use and population data. *GISci. Remote Sens.* **2015**, *52*, 765–780. [[CrossRef](#)]
57. Waibel, A.; Hanazawa, T.; Hinton, G.; Shikano, K.; Lang, K.J. Phoneme recognition using time-delay neural networks. In *Backpropagation*; Psychology Press: London, UK, 2013; pp. 35–61.
58. Yamashita, R.; Nishio, M.; Do, R.K.G.; Togashi, K. Convolutional neural networks: An overview and application in radiology. *Insights Imaging* **2018**, *9*, 611–629. [[CrossRef](#)]
59. Zuo, R.; Xiong, Y.; Wang, J.; Carranza, E.J.M. Deep learning and its application in geochemical mapping. *Earth Sci. Rev.* **2019**, *192*, 1–14. [[CrossRef](#)]
60. Hoseinzade, E.; Haratizadeh, S. CNNpred: CNN-based stock market prediction using a diverse set of variables. *Expert Syst. Appl.* **2019**, *129*, 273–285. [[CrossRef](#)]
61. Kennedy, J.; Eberhart, R. Particle Swarm Optimization. In Proceedings of the ICNN'95-International Conference on Neural Networks, Perth, WA, Australia, 27 November–1 December 1995; IEEE: New York, NY, USA, 1995; pp. 1942–1948.
62. Li, Y.; Yu, K.; Liang, J.; Yue, C.; Qiao, K. A landscape-aware particle swarm optimization for parameter identification of photovoltaic models. *Appl. Soft Comput.* **2022**, *131*, 109793. [[CrossRef](#)]
63. Pace, F.; Santilano, A.; Godio, A. A review of geophysical modeling based on particle swarm optimization. *Surv. Geophys.* **2021**, *42*, 505–549. [[CrossRef](#)]

64. Engelbrecht, A. Computational intelligence an introduction. *IEEE Trans. Neural Netw.* **2005**, *16*, 780.
65. Martinez, C.M.; Cao, D. *iHorizon-Enabled Energy Management for Electrified Vehicles*; Butterworth-Heinemann: Oxford, UK, 2018.
66. Chollet, F. *Deep Learning with Python*; Simon and Schuster: New York, NY, USA, 2021.
67. Zaidi, A. Predicting wildfires in Algerian forests using machine learning models. *Heliyon* **2023**, *9*, e18064. [[CrossRef](#)] [[PubMed](#)]
68. Zaïdi, A. Accurate IoU computation for rotated bounding boxes in R^2 and R^3 . *Mach. Vis. Appl.* **2021**, *32*, 114. [[CrossRef](#)]
69. Chang, Y.; Zhu, Z.; Bu, R.; Chen, H.; Feng, Y.; Li, Y.; Hu, Y.; Wang, Z. Predicting fire occurrence patterns with logistic regression in Heilongjiang Province, China. *Landsc. Ecol.* **2013**, *28*, 1989–2004. [[CrossRef](#)]
70. Vilar del Hoyo, L.; Martín Isabel, M.P.; Martínez Vega, F.J. Logistic regression models for human-caused wildfire risk estimation: Analysing the effect of the spatial accuracy in fire occurrence data. *Eur. J. For. Res.* **2011**, *130*, 983–996. [[CrossRef](#)]
71. Bisquert, M.; Caselles, E.; Sánchez, J.M.; Caselles, V. Application of artificial neural networks and logistic regression to the prediction of forest fire danger in Galicia using MODIS data. *Int. J. Wildland Fire* **2012**, *21*, 1025–1029. [[CrossRef](#)]
72. Guo, F.; Wang, G.; Su, Z.; Liang, H.; Wang, W.; Lin, F.; Liu, A. What drives forest fire in Fujian, China? Evidence from logistic regression and Random Forests. *Int. J. Wildland Fire* **2016**, *25*, 505–519. [[CrossRef](#)]
73. Ma, W.; Feng, Z.; Cheng, Z.; Chen, S.; Wang, F. Identifying forest fire driving factors and related impacts in China using random forest algorithm. *Forests* **2020**, *11*, 507. [[CrossRef](#)]
74. Singh, K.R.; Neethu, K.; Madhurekaa, K.; Harita, A.; Mohan, P. Parallel SVM model for forest fire prediction. *Soft Comput.* **2021**, *3*, 100014. [[CrossRef](#)]
75. Pacheco, A.d.P.; Junior, J.A.d.S.; Ruiz-Armenteros, A.M.; Henriques, R.F.F. Assessment of k-nearest neighbor and random forest classifiers for mapping forest fire areas in central portugal using landsat-8, sentinel-2, and terra imagery. *Remote Sens.* **2021**, *13*, 1345. [[CrossRef](#)]
76. Pourtaghi, Z.S.; Pourghasemi, H.R.; Rossi, M. Forest fire susceptibility mapping in the Minudasht forests, Golestan province, Iran. *Environ. Earth Sci.* **2015**, *73*, 1515–1533. [[CrossRef](#)]
77. Abedi Gheshlaghi, H. Using GIS to develop a model for forest fire risk mapping. *J. Indian Soc. Remote Sens.* **2019**, *47*, 1173–1185. [[CrossRef](#)]
78. Mavrovouniotis, M.; Li, C.; Yang, S. A survey of swarm intelligence for dynamic optimization: Algorithms and applications. *Swarm Evol. Comput.* **2017**, *33*, 1–17. [[CrossRef](#)]
79. Tian, J.; Li, M.; Chen, F.; Feng, N. Learning subspace-based RBFNN using coevolutionary algorithm for complex classification tasks. *IEEE Trans. Neural Netw. Learn. Syst.* **2016**, *27*, 47–61. [[CrossRef](#)]
80. Nickabadi, A.; Ebadzadeh, M.M.; Safabakhsh, R. A novel particle swarm optimization algorithm with adaptive inertia weight. *Appl. Soft Comput.* **2011**, *11*, 3658–3670. [[CrossRef](#)]
81. Lee, C.-M.; Ko, C.-N. Time series prediction using RBF neural networks with a nonlinear time-varying evolution PSO algorithm. *Neurocomputing* **2009**, *73*, 449–460. [[CrossRef](#)]
82. Camci, E.; Kripalani, D.R.; Ma, L.; Kayacan, E.; Khanesar, M.A. An aerial robot for rice farm quality inspection with type-2 fuzzy neural networks tuned by particle swarm optimization-sliding mode control hybrid algorithm. *Swarm Evol. Comput.* **2018**, *41*, 1–8. [[CrossRef](#)]
83. Xue, X.; Tsai, P.-W. Integrating Energy Smart Grid’s ontologies through multi-objective particle swarm optimization algorithm with competitive mechanism. *Sustain. Energy Technol. Assess.* **2022**, *53*, 102442. [[CrossRef](#)]
84. Kiranyaz, S.; Ince, T.; Gabbouj, M. Real-time patient-specific ECG classification by 1-D Convolutional Neural Networks. *IEEE Trans. Biomed. Eng.* **2016**, *63*, 664–675. [[CrossRef](#)]
85. Abdeljaber, O.; Avci, O.; Kiranyaz, S.; Gabbouj, M.; Inman, D.J. Real-time vibration-based structural damage detection using one-dimensional convolutional neural networks. *J. Sound Vib.* **2017**, *388*, 154–170. [[CrossRef](#)]
86. Bui, D.T.; Tsangaratos, P.; Nguyen, V.-T.; Liem, N.V.; Trinh, P.T. Comparing the prediction performance of a Deep Learning Neural Network model with conventional machine learning models in landslide susceptibility assessment. *Catena* **2020**, *188*, 104426. [[CrossRef](#)]
87. Levin, N.; Kyba, C.C.M.; Zhang, Q.; Sánchez de Miguel, A.; Román, M.O.; Li, X.; Portnov, B.A.; Molthan, A.L.; Jechow, A.; Miller, S.D.; et al. Remote sensing of night lights: A review and an outlook for the future. *Remote Sens. Environ.* **2020**, *237*, 111443. [[CrossRef](#)]
88. Navara, K.J.; Nelson, R.J. The dark side of light at night: Physiological, epidemiological, and ecological consequences. *J. Pineal. Res.* **2007**, *43*, 215–224. [[CrossRef](#)]
89. Roman, M.O.; Stokes, E.C. Holidays in lights: Tracking cultural patterns in demand for energy services. *Earths Future* **2015**, *3*, 182–205. [[CrossRef](#)]
90. Pham, B.T.; Jaafari, A.; Avand, M.; Al-Ansari, N.; Dinh Du, T.; Yen, H.P.H.; Phong, T.V.; Nguyen, D.H.; Le, H.V.; Mafi-Gholami, D.; et al. Performance evaluation of machine learning methods for forest fire modeling and prediction. *Symmetry* **2020**, *12*, 1022. [[CrossRef](#)]
91. Zhao, N.; Liu, Y.; Cao, G.; Samson, E.L.; Zhang, J. Forecasting China’s GDP at the pixel level using nighttime lights time series and population images. *GISci. Remote Sens.* **2017**, *54*, 407–425. [[CrossRef](#)]

Disclaimer/Publisher’s Note: The statements, opinions and data contained in all publications are solely those of the individual author(s) and contributor(s) and not of MDPI and/or the editor(s). MDPI and/or the editor(s) disclaim responsibility for any injury to people or property resulting from any ideas, methods, instructions or products referred to in the content.